Dual Diffusion and Finite Mass Exchange Model for Adsorption Kinetics in Activated Carbon

D. D. Do and K. Wang
Dept. of Chemical Engineering, University of Queensland, St. Lucia, QLD 4072, Australia

A model allowing for the finite mass exchange between the two phases is proposed for the description of adsorption kinetics in activated carbon. This model based on Do's earlier structural model for activated carbon involves three mass-transfer processes: pore diffusion, adsorbed phase diffusion, and finite mass interchange between the fluid and adsorbed phases. The solid phase is heterogeneous, which is characterized by the micropore size distribution. The interaction between the adsorbate molecule and the micropore is calculated from the Lennard-Jones potential theory. The model developed for nonpolar adsorbates is tested with the experimental data of seven adsorbates (paraffin gases, aromatics, carbon dioxide, and sulfur dioxide) on pellets of different shapes and sizes and at various operating conditions. The finite kinetics play an important role in the overall kinetics. Failure to account for this finite kinetics makes the model unable to describe correctly the desorption behavior, since under such conditions, the ability of the particle to release adsorbed molecules is dictated mostly by the resistance at the pore mouth of the micropore.

Introduction

Adsorption kinetics on microporous materials such as activated carbon and other carbon related materials is important to the understanding of the rate of adsorption as well as the selectivity in many practical processes (Yang, 1987). Because of the combined effect of the complicated structure of activated carbon and its complex nature, the surface diffusion which plays a very important role in the overall kinetics remains a challenging problem. Modeling of surface diffusion in activated carbon still contains a certain degree of empiricism. What we can do, however, is to develop a model which could account for the heterogeneity in surface diffusion, as well as the pore mouth behavior of micropore, which results in the finite mass exchange between the bulk and the adsorbed phases. No matter what mathematical models are proposed for describing adsorption kinetics, parameters such as particle size, bulk concentration, and operating conditions of pressure and temperature must be fully accounted for (Gray and Do, 1990, 1991; Do and Hu, 1993; Hu and Do, 1993). It is the objective of this article to develop a general model for the description of adsorption kinetics in activated carbon based on its structural characteristics.

Correspondence concerning this article should be addressed to D. D. Do.

Experimental observations of adsorption kinetics

If a mathematical model is to carry its useful role in simulating or predicting adsorption/desorption in activated carbon, it must be able to describe the following facts which have been observed experimentally in a large number of experiments (Do, 1997):

(1) When a particle is large, the adsorption time scale is proportional to the square of the particle radius (Gray and Do, 1990). This time scale becomes independent of the particle size when the particle is small.

(2) The approach to equilibrium is faster when the bulk concentration increases.

(3) The sorption rate decreases as the temperature increases, but the time to approach equilibrium is shorter due to the lesser amount adsorbed at high temperature.

(4) The sorption rate into the particle exceeds the rate purely described by pore diffusion, suggesting that there is an additional transport mechanism. This additional flux is contributed to by the diffusion of the adsorbed species via the adsorbed phase.

(5) The observed surface diffusivity increases strongly with the adsorbed concentration.

(6) Except for some adsorbates, such as low paraffins, the adsorption equilibrium between the fluid and adsorbed

phases cannot be described by the simple Langmuir equation.

(7) The adsorbed phase is heterogeneous as observed by the electron microscope or by spectroscopy methods.

(8) The desorption time scale is longer than the adsorption time scale and the desorption curve exhibits a very long tail, indicating that there exist sites of varying energy of interaction and high energy sites release molecules at a rate much lower than low energy sites.

Theory

In this diffusion model, both the adsorption equilibria and kinetics are dictated by the size distribution of the slit-shaped channels (micropores) of activated carbon, and this distribution is considered as the main source of surface heterogeneity in physical adsorption. Thus in the present study, the concept of micropore size distribution (MPSD) is employed in the analysis of adsorption equilibria as well as kinetics to account for the heterogeneity.

Adsorption equilibria and MPSD

Since the diffusion mechanism in a structural model is influenced by the microporous structure, it is important to obtain the reliable MPSD which characterizes the activated carbon. In this section, we will study the system heterogeneity in terms of the structural heterogeneity and present the way of obtaining this MPSD from the simultaneous utilization of adsorption equilibrium data of many adsorbates collected at a range of temperature.

Microporous Structure and Adsorption Energetic Heterogeneity. The general approach towards the surface heterogeneity is to treat is as energetically patch-wise, that is, sites with the same adsorption energy are grouped together. The overall isotherm then can be expressed as the integral of the local isotherm $C_\mu(E)$ (mol/m^3) over the whole energy distribution range (Myers, 1984), that is,

$$C_\mu = \int_{E_{\min}}^{E_{\max}} C_\mu(E) F(E) dE \tag{1a}$$

where $F(E)$ is the energy distribution function, and $E_{\min}$ and $E_{\max}$ are the lower and upper limits of the energy distribution, respectively. For adsorption of nonpolar adsorbates such as paraffins, the interaction between the adsorbate molecule and the pore mainly comes from the dispersive force; hence, the energetic heterogeneity of the system arises due to the structural heterogeneity, or the distribution of slit-shaped micropores. The equivalence of Eq. 1a written in terms of MPSD represented by $f(r)$, is given by

$$C_\mu = \int_{r_1}^{r_2} C_\mu(r) f(r) dr \tag{1b}$$

where r_1 (Å) is the lower limit of pore half width accessible to the adsorbate molecule and r_2 is the upper limit of the micropore range. Although Eqs. 1a and 1b are mathematically equivalent, Eq. 1b is more fundamentally based. In addition, the energy distribution $F(E)$, which is induced by the MPSD, may not follow any particular type of distribution function while the pore-size distribution $f(r)$ is controlled by the random processes of carbonization and activation in the manufacturing stage of activated carbon. Hence, assuming a distribution function for $f(r)$ is theoretically sound and more reasonable than assuming a distribution function for $F(E)$. Once $f(r)$ is known, the $F(E)$ is related to $f(r)$ by

$$F(E) = \frac{f(r)}{dE(r)/dr} \tag{1c}$$

where $E(r)$ is the local adsorption energy, (J/mol) which is taken as the negative of the adsorption potential minimum inside the pores with half width r. To obtain this functional dependence $E(r)$, we consider two models for the slit-shaped micropores of activated carbon. In one model, each of the micropore walls is assumed to be a single lattice layer of infinite extent, while in the other the pore walls are assumed to be made of parallel lattice layers with sublattice layers separated by a distance Δ. The potential energy of an adsorbate molecule interacting with the micropore is given by the 10-4 potential and the 10-4-3 potential for the first model and the second model, respectively (Steele, 1974; Jagiello, 1996)

10-4 potential

$$\varphi_k(z,r) = \frac{5}{3}\epsilon_k^* \left[\frac{2}{5}\left(\frac{\sigma_{sk}}{2r-z}\right)^{10} + \frac{2}{5}\left(\frac{\sigma_{sk}}{z}\right)^{10} - \left(\frac{\sigma_{sk}}{2r-z}\right)^{4} - \left(\frac{\sigma_{sk}}{z}\right)^{4} \right] \tag{2a}$$

10-4-3 potential

$$\varphi_k(z,r) = \frac{5}{3}\epsilon_k^* \left[\frac{2}{5}\left(\frac{\sigma_{sk}}{2r-z}\right)^{10} + \frac{2}{5}\left(\frac{\sigma_{sk}}{z}\right)^{10} - \left(\frac{\sigma_{sk}}{2r-z}\right)^{4} - \left(\frac{\sigma_{sk}}{z}\right)^{4} - \left(\frac{\sigma_{sk}^4}{3\Delta(0.61\Delta+z)^3}\right) - \left(\frac{\sigma_{sk}^4}{3\Delta(0.61\Delta+2r-z)^3}\right) \right] \tag{2b}$$

where ϵ_k^* is given by

$$\epsilon_k^* = \frac{6}{5}\pi n \sigma_{sk}^2 \epsilon_{sk} \tag{2c}$$

$$\epsilon_k^* = \frac{6}{5}\pi \rho_s \Delta \sigma_{sk}^2 \epsilon_{sk} \tag{2d}$$

for the 10-4 potential and 10-4-3 potential, respectively. The parameter z (Å) is the distance between the adsorbate molecule and one of the pore walls, n (atoms/nm^2) is the number of site per unit area of lattice layer (38.2 nm^{-2}), ρ_s (atoms/nm^2) is the number density of carbon (144 nm^{-3}), and Δ is the spacing between sublattice layers (0.335 nm) (Steele, 1974). The parameters ϵ_{sk} and σ_{sk} are obtained from the Lorentz-Berthelot rule

$$\epsilon_{sk} = \sqrt{\epsilon_{ss}\epsilon_{kk}} \tag{2e}$$

$$\sigma_{sk} = \frac{\sigma_{ss} + \sigma_{kk}}{2} \tag{2f}$$

Solving Eqs. 2 for minimums and taking the negative of this minimum potential as the interaction energy between the adsorbate molecule and the micropore, we will obtain the functional dependence between the interaction adsorption energy E (J/mol) and the pore half width r.

MPSD and the overall isotherm equation

We assume that the adsorbate-adsorbate interaction is not as strong as the adsorbate-adsorbent interaction, and hence the local isotherm in the integrand of Eq. 1b can be assumed to follow the Langmuir equation relating the adsorbed phase concentration in the pores with half width r to the gas phase concentration C as follows

$$C_\mu(r) = C_{\mu s}(T)\frac{Cb(r)}{1+Cb(r)} \tag{3a}$$

where $b(r)$ is the local adsorption affinity, defined as

$$b(r) = b_\infty \exp\left(\frac{E(r)}{R_g T}\right) \tag{3b}$$

The b_∞ is the adsorption affinity at infinite temperature. For various species, it can be represented by

$$b_\infty = \frac{\beta}{\sqrt{MT}} \tag{3c}$$

Equation 3c is derived by assuming that the rate of adsorption is related to the molecular collision rate toward the surface (or specifically the micropore mouth) and this collision rate is inversely proportional to the square root of molecular weight and the square root of temperature (Do and Do, 1996). The affinity parameter β is assumed to be solid specific and independent of adsorbate. The maximum adsorption capacity of each species $C_{\mu s}$ (mol/m^3) has following temperature dependence

$$C_{\mu s}(T) = C^0_{\mu s}\exp[\delta(T_0 - T)] \tag{3d}$$

where $C^0_{\mu s}$ (mol/m^3) is the maximum adsorption capacity at reference temperature T_0(K), and δ(K^{-1}) is the thermal expansion coefficient.With regard to the micropore size distribution, we will assume in this work that it will follow the form of the non-negative Gamma distribution function

$$f(r) = \frac{q^{\gamma+1}r^\gamma e^{-qr}}{\Gamma(\gamma+1)} \tag{4}$$

where q and γ are distribution parameters characterizing the adsorbent structure. q is the Gamma distribution parameter (Å^{-1}). With all the functions and parameters defined, the overall isotherm of Eq. 1b can be readily expressed as

$$C_\mu = \int_{r_1}^{r_2} C_{\mu s}(T)\frac{Cb(r)}{1+Cb(r)}\frac{q^{\gamma+1}r^\gamma e^{-qr}}{\Gamma(\gamma+1)}dr \tag{5}$$

where r_1 is the minimum pore half width accessible to adsorbate molecule, which is obtained from the pore that has the same adsorption potential energy as that of a single lattice layer. The value of r_1 varies for species with different diameters and it can be obtained by numerically solving Eqs. 2. The upper limit r_2 is the maximum pore half width, which has no limit in general, but is taken as $3.5\sigma_{sk}$ for convenience in this study since pores having a size larger than this will have low interaction energy and hence low adsorption density.

Equation 5 is the general isotherm equation applicable to all species in this study. By optimizing the model equation with the multiple temperature isotherm data of all species simultaneously, the intrinsic MPSD parameters q and γ together with the isotherm parameters can be derived. It should be pointed out that the approach used here is theoretically more sound than our previous study in which only the 10–4 potential is considered and the size difference between different adsorbates is neglected (Do and Wang, 1997).

Mass interchange between fluid and adsorbed phase

In the structural diffusion model proposed by Do (1996), the diffusion of adsorbate molecules within the graphitic layers is accompanied by the continuous penetration into and evaporation from these layers. These microscopic processes can be viewed macroscopically as the lumped finite mass interchange process between the fluid and adsorbed phases. The rates of adsorption and desorption between two phases are assumed to follow the Langmuir kinetics, that is

$$R_{net} = (k_a C_{\mu s})C - (k_a C + k_d)C_\mu \tag{6}$$

The rate constants k_a and k_d are lumped parameters, lumping various microprocesses, and are regarded as empirical constants in this work. k_a is the adsorption rate constant {1/s/(mol/m^3)}, and k_d is the desorption rate constant (s^{-1}). The ratio of these two constants is the adsorption affinity b, which is determined from the equilibria studies; hence, from the kinetics study perspective only one parameter is required (either k_a or k_d) to describe the finite mass interchange process. The form of Langmuir kinetic (Eq. 6) may not be correct in the description of finite mass exchange between the two phases in activated carbon, but it is more than adequate to explain a number of kinetics observations in our laboratories. If the finite mass exchange is governed by Eq. 6, the adsorption time constant is given by

$$t^0_{\text{ads}} = \frac{1}{k_a C + k_d} \tag{7}$$

In adsorption mode with a bulk environment of concentration C, Eq. 7 represents the adsorption time constant, which shows that the higher the bulk concentration is the lower is

the adsorption time, as many adsorption experiments have shown. However, this observation can also be explained by the model of pore diffusion with a favorable adsorption isotherm. This means that an observation of lower adsorption time with an increase in the bulk concentration could point to:

(a) finite Langmuir kinetics type and/or

(b) pore and/or surface diffusion with a favorable adsorption isotherm.

The delineation of these two mechanisms is possible when we consider the desorption. Desorption curves of many adsorbates from activated carbon exhibit a long tail, indicating a slower release of the molecule from the adsorbed phase. This is attributed to the finite kinetics between the two phases since such a slow release cannot be explained by the pore/surface diffusion model. For the structurally heterogeneous adsorbent considered in this article, the rate constants for adsorption and desorption in Eq. 6 are functions of local pore size. Thus, for each pore size, the mass interchange kinetics equation is

$$\frac{\partial C_\mu(r)}{\partial t} = k_{ads}(r)C[C_{\mu s} - C_\mu(r)] - k_{des}(r)C_\mu(r) \quad (8)$$

The desorption rate constant follows the Arrhenius relation

$$k_{des}(r) = k_{des,\infty} \exp\left(-\frac{E(r)}{R_g T}\right) \quad (9)$$

where $k_{des,\infty}$ is taken to be independent of pore size. The pore size dependence is reflected in the desorption energy $E(r)$, which is the interaction energy between the adsorbate molecule and the micropore of half width r.

Rate of Diffusion of the adsorbed species

So far, the kinetic behaviors of adsorbed phase are investigated in the absence of any mobility of the adsorbate in both free and adsorbed forms. When the adsorbed species is mobile, the diffusion of the adsorbed species will contribute to the overall mass transfer of molecules into the particle interior or out of the particle. Because the mass exchange rate between the gas and adsorbed phases is finite, the two phases are not in local equilibrium. By taking the chemical potential as the driving force for surface diffusion and defining a hypothetical gas phase concentration C^*, which is in local equilibrium with the adsorbed phase

$$C^* = \frac{C_\mu(r)}{b(r)[C_{\mu s} - C_\mu(r)]} \quad (10)$$

The overall surface phase flux $\langle J_\mu \rangle$ (mol/m^2/s) can be expressed as

$$\langle J_\mu \rangle = \int_{r_{min}}^{r_{max}} J_\mu(r) f(r) dr = -\int_{r_{min}}^{r_{max}} \left[D_\mu^0(r) \frac{C_{\mu s}}{C_{\mu s} - C_\mu(r)} \frac{\partial C_\mu(r)}{\partial Z} \right] f(r)\, dr \quad (11)$$

where

$$D_\mu^0 = D_{\mu\infty}^0 \exp\left(-\frac{aE(r)}{R_g T}\right) \quad (12)$$

is the local surface diffusivity at zero loading, $D_{\mu\infty}^0$ (m^2/s) is the surface diffusivity at infinite temperature, a is the ratio of activation energy for surface diffusion to the adsorption energy (0.5), and Z (m) is the particle coordinate. The lower and upper limits for integration (r_{min} and r_{max}) are defined in the same way as r_1 and r_2.

Gas phase diffusion flux

The flux of gas-phase diffusion in macropore or mesopore is represented by the Fickan diffusion, that is

$$J_p = -D_p \frac{\partial C}{\partial Z} \quad (13)$$

where D_p (m^2/s) is the pore diffusivity, which is calculated from the combination of molecular and Knudsen diffusion processes (Ruthven, 1984; Do and Hu, 1993).

Mass balance equation

Overall Mass Balance Equation. Having obtained the necessary expressions of the finite mass interchange rate, gas-phase diffusion flux, and local surface flux, the overall mass balance equation of a particle with geometric factor s (of pellet: 0,1, 2, for slab, cylinder and sphere) can be expressed in terms of MPSD as

$$\epsilon \frac{\partial C}{\partial t} + (1-\epsilon) \frac{\partial}{\partial t} \left\{ \int_{r_{min}}^{r_{max}} C_\mu(r) f(r) dr \right\} = \epsilon D_p \frac{1}{Z^s} \frac{\partial}{\partial Z} \left(Z^s \frac{\partial C}{\partial Z} \right) + (1-\epsilon) \frac{1}{Z^s} \frac{\partial}{\partial Z} \times \left\{ Z^s \int_{r_{min}}^{r_{max}} \left[D_\mu^0(r) \frac{C_{\mu s}}{C_{\mu s} - C_\mu(r)} \frac{\partial C_\mu(r)}{\partial Z} \right] f(r) dr \right\} \quad (14)$$

This equation simply states that the accumulation of mass in both free and adsorbed forms (LHS) is balanced by the diffusion rates into the particle of the gas (first term in RHS) and the adsorbed species. To complete this mass balance description, the mass balance around the adsorbed phase should be specified.

Adsorbed Phase Mass Balance Equation. The mass balance equation of the adsorbed phase over the pores with the half width r is

$$\frac{\partial C_\mu(r)}{\partial t} = \frac{1}{Z^s} \frac{\partial}{\partial Z} \left[Z^s D_\mu^0(r) \frac{C_{\mu s}}{C_{\mu s} - C_\mu(r)} \frac{\partial C_\mu(r)}{\partial Z} \right] + [k_a C + k_d(r)] \left[C_{\mu s} \frac{b(r)C}{1 + b(r)C} - C_\mu(r) \right] \quad (15)$$

Equations 14 and 15 define the sorption kinetics in activated carbon. Solving these equations with appropriate boundary conditions and initial condition, we will obtain the concentration distributions for the fluid and adsorbed phases in the particle. Knowing these distributions, the average concentrations, the diffusion fluxes, and the fractional uptake can be calculated.

Boundary Conditions of the Model Equations. The pertinent boundary conditions and initial conditions for the model equations are

$$Z = 0, \quad \frac{\partial C}{\partial Z} = 0 \tag{16a}$$

$$Z = R, \quad \epsilon J_p + (1-\epsilon)\int_{r_{\min}}^{r_{\max}} J_\mu(r) f(r) dr = k_m (C - C_b) \tag{16b}$$

$$t = 0, \quad C = C_0, \quad C_{\mu 0} = \int_{r_{\min}}^{r_{\max}} C_{\mu s} \frac{b(r) C_0}{1 + b(r) C_0} f(r) dr \tag{17}$$

where C_b is the bulk phase concentration (mol/m^3) and C_0 (mol/m^3) is the initial concentration of adsorbate.

Special Cases

We have presented the general mathematical model for sorption kinetics in activated carbon, which is based on the structural properties of the adsorbent and allows for three mass-transfer mechanisms coexisting in the system. In the model development no particular assumptions are made regarding the adsorption energy distribution, operating conditions, and so on. However, when certain criteria are met, this model can reduce (degenerate) to many simpler models used in the study of adsorption kinetics such as the homogeneous model, energy bi-dispersed model, or the model for compact solids. To save space, we show only in the following section one of these special cases, that is the fast sorption kinetics compared with diffusion rate.

Fast Adsorption/Desorption Kinetics Compared to Diffusions. When local adsorption equilibrium conditions prevail, the rates of adsorption and desorption are much faster than the diffusion rates in the fluid as well as in the adsorbed phase. Since the mobility of molecules into the particle interior is low, the rate of mass interchange between the two phases is fast enough to ensure a local equilibrium to establish. As a result, at any point within the particle, the rate of adsorption is the same as the rate of desorption, that is the fluid concentration and the adsorbed phase concentration are related to each other, according to

$$C_\mu(r) = C_\mu^* = C_{\mu s} \frac{b(r) C}{1 + b(r) C} \tag{18a}$$

With this local equilibrium, the concentration in the adsorbed phase is related to that in the gas phase and so are their respective concentration gradients, that is

$$\frac{\partial C_\mu(r)}{\partial Z} = \frac{b(r) C_{\mu s}}{[1 + b(r) C]^2} \frac{\partial C}{\partial Z} \tag{18b}$$

Thus, if there exists a concentration gradient in the gas phase, there also exists a gradient in the adsorbed phase which is algebraically related to the gradient of the gas-phase species according to Eq. 18a. The algebraic relation between the two concentrations in Eq. 18a means that if there is a sudden change in the concentration of one phase, the concentration and the gradient of the other phase will change accordingly with no time delay. It is also noted from Eq. 18b that the higher the gas-phase concentration, the smaller is the gradient in the adsorbed phase concentration. This suggests that the adsorbed phase diffusion is less important at high concentrations.

The mass balance equation of the system is then given as in Eq. 14, with $C_\mu(r)$ in that equation being replaced by that described by Eq. 18. We substitute Eq. 18 into Eq. 14, and obtain the following mass balance equation written in terms of the gas-phase concentration

$$[\epsilon + (1-\epsilon) H(C)] \frac{\partial C}{\partial t} = \frac{1}{Z^s} \frac{\partial}{\partial Z} \left[Z^s D_c(C) \frac{\partial C}{\partial Z} \right] \tag{19}$$

where

$$H(C) = \int_{r_{\min}}^{r_{\max}} \frac{C_{\mu s} b(r)}{[1 + b(r) C]^2} f(r) dr \tag{20a}$$

$$D_c(C) = \epsilon D_p + (1-\epsilon) \int_{r_{\min}}^{r_{\max}} D_\mu^0(r) \frac{C_{\mu s} b(r)}{[1 + b(r) C]} f(r) dr \tag{20b}$$

Equations 19 and 20 have the same mechanism as the heterogeneous macropore, surface, diffusion model (HMSD) proposed by Do et al. (1993) for large particles. Solving this set of equations and then comparing this result with that obtained in the general case of finite adsorption kinetics, we can gather information about the role the finite adsorption kinetics would play in the sorption kinetics.

Solution Methodology

The model equations for the general case, Eqs. 14 and 15, are coupled partial differential equations. By defining the nondimensional variables and parameters as listed in the Appendix, the model equations are cast into nondimensional forms and then converted into ODEs by an orthogonal collocation technique. The final form of the model is solved numerically by the ODE solver in MATLAB.

Experiment

Adsorption equilibria data were collected using a high-accuracy volumetric rig. Adsorption isotherms of seven species on Ajax activated carbon are measured, they are: (1) ethane, (2) propane, (3) *n*-butane, (4) benzene, (5) toluene, (6) carbon dioxide, (7) sulfur dioxide. For each species, adsorption isotherms at several temperatures (≥ 3) were measured (Do and Do, 1996). The single component adsorption/desorption kinetics on Ajax carbon were measured on a differential adsorber bed rig (DAB), under various conditions such as different temperatures, pellet length/geometry and bulk concentrations (Do, 1997). High purity nitrogen is used as the

diluting gas in the bulk phase. The detailed setup of volumetric and DAB rigs as well as their related experimental procedures are also described in Do (1997).

Results and Discussion

Equilibria and MPSD

The extensive experimental isotherm data of seven species are employed simultaneously in Eq. 5 to derive the MPSD parameters for the carbon structure. The reference temperature for adsorption capacity $C^0_{\mu s}$ is chosen as 273 K. For the purpose of calculation, the molecular properties and experimental temperatures at which equilibria data are collected are listed in Table 1.

As a result of the fitting between the experimental data and the theoretical model using the 10-4-3 potential, the model fitting (solid lines) and experimental data (symbols) are shown in Figure 1 for each species and the optimized MPSD parameters for the Gamma distribution are

$$q = 16.9\ (\text{Å}^{-1})$$

$$\gamma = 77.4$$

$$\beta = 1.001 \times 10^{-3}\ [\text{m}^3 \cdot \text{mol}^{-1} (\text{g} \cdot \text{K/mol})^{1/2}]$$

and the optimized isotherm parameters for various adsorbates are listed in Table 2a. On the other hand, using the 10-4 potential in the theoretical equation, we obtain the following parameters for the Gamma distribution:

$$q = 18.0\ (\text{Å}^{-1})$$

$$\gamma = 82.8$$

$$\beta = 0.894 \times 10^{-3}\ [\text{m}^3 \cdot \text{mol}^{-1}\ (\text{g} \cdot \text{K/mol})^{1/2}]$$

and the parameters for each adsorbate are shown in Table 2b. The model fitting is shown in Figure 1 as the dotted lines.

It is seen in Figures 1 that using either potential equation (10-4 or 10-4-3) the overall isotherm model is able to simulate the adsorption equilibria of each species over a wide temperature range. The MPSDs derived from both 10-4-3 and 10-4 potential are shown in Figure 2, and we also show the accessibility cut off of each species in the same figure. It is seen that the derived MPSDs from both potential equations are strikingly similar. The average micropore width of Ajax carbon is about 9.0 Å, which falls in the range of pore size determined by experimental methods for activated carbon (Innes et al., 1989). With the derived MPSDs, the adsorption energy distributions for each species are converted according to Eq. 1c and the average adsorption energy E_{mean} of each species is calculated and tabulated in Tables 2a and 2b for each potential. We note in Tables 2 that, for either potential, the minimum interactive energy of the adsorbate molecule with single lattice layer ϵ^*_k(J/mol) and the average adsorption energy E_{mean} increases with the carbon number for a given class of adsorbate family (ethane, propane, butane). Aromatics have higher ϵ^*_k and E_{mean} than those of paraffins, with toluene being the stronger adsorbing species than benzene. We also noted in Tables 2 that the derived saturation capacities at 273 K for SO_2 and CO_2 are unreasonably high, which is possibly due to fact that, for polar adsorbates, the dispersive interaction assumed in this model may not be enough to account for the interaction between adsorbate and carbon surface.

Table 1. Isotherm Temperatures and Molecular Properties

Species	Ethane	Propane	Butane	Benzene	Toluene	CO_2	SO_2
M (g/mol)	30	44	58	78	92	44	64
σ_k (Å)	3.9	4.3	4.3	3.7	3.82	3.3	3.6
T (K)	283,303 333	283,303 333	283,303 333,423	303,333 363,423	303,333 363	298,323 373	298,323 373

Figure 3 shows the optimized ϵ^*_k in Table 2a and 2b against their theoretical values calculated from Eq. 2c for 10-4 potential and Eq. 2d for 10-4-3 potential, respectively, by using the parameters from Bird (1962) and Steele (1974). It is very interesting to note that the optimal and the theoretical values are very comparable to each other for either potential with the results from 10-4-3 potential presenting better compatibility.

The isotherm parameters and MPSD parameters are then used in the study of adsorption kinetics.

Adsorption kinetics

The adsorption kinetics experiments are carried out on the DAB rig with the bulk gas-phase pressure being kept constant at 1 atm. Extensive single component uptake curves are measured under different operating conditions and/or pellet sizes for each species, which are employed later to check the model's applicability and to ensure the reliability of the simulation results. To further examine the theory and some assumptions of this finite kinetics model (hereafter referred to as FK model), the HMSD model, which is a special case of the FK model (discussed in the Special Cases subsection) and has been used in the past studies, is also employed in the simulation using the same MPSD and isotherm parameters. With the gas-phase diffusivity calculated from the combined molecular and Knudsen diffusion process, the kinetics parameters to be optimized in the FK model are the surface diffusivity at zero loading and infinite temperature $D^0_{\mu\infty}$ and the rate constant of adsorption k_a. For the HMSD model, which assumes the instant equilibrium between the fluid and adsorbed phases, the only kinetics parameter to be optimized is the surface diffusivity at zero loading and infinite temperature $D^0_{\mu\infty}$. By comparing the simulation results in these two models, it is possible for us to investigate the role of finite mass exchange in the overall kinetics and to obtain some criteria in model selection. This study has several improvements compared with our previous study (Do and Wang, 1997) for the same kinetics systems: (1) The MPSD derived takes into account the size difference between adsorbates; (2) two configurations of the silt-shaped micropores are considered; (3) more experimental kinetics data are used in the simulation; (4) the implications of the model and the derived kinetics parameters are further investigated through the comparison between the FK and HMSD models.

Ethane. We start our discussion of adsorption kinetics with ethane adsorption on Ajax activated carbon. The kinet-

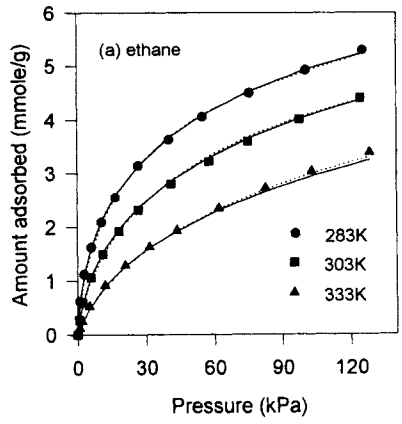

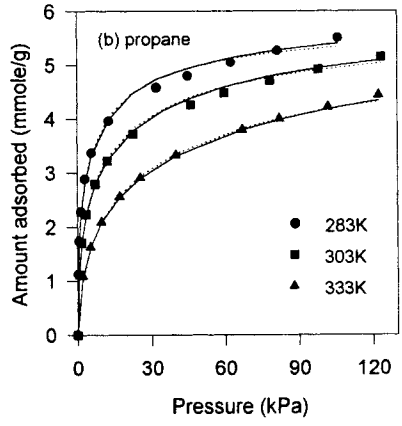

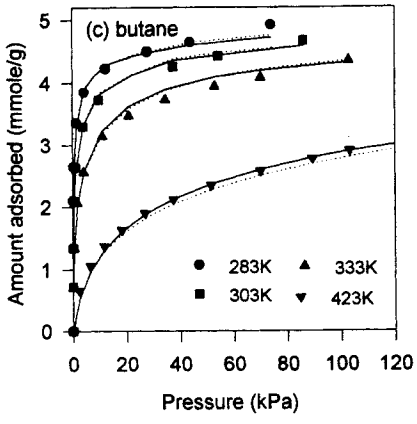

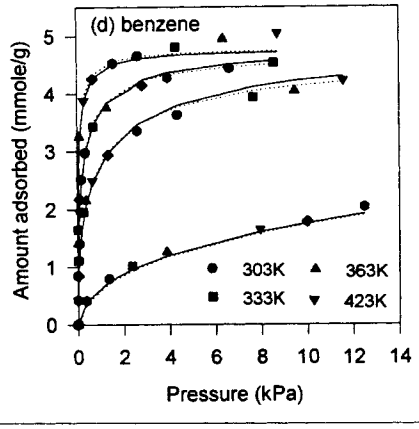

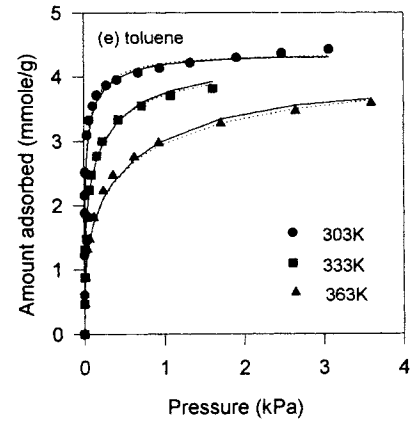

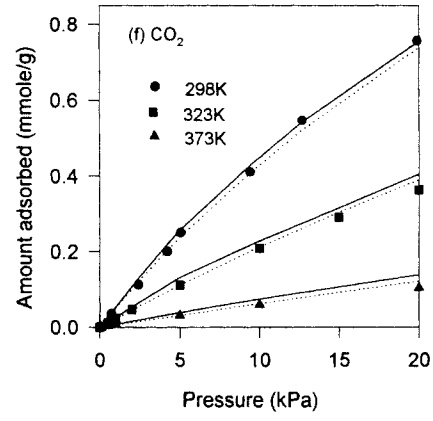

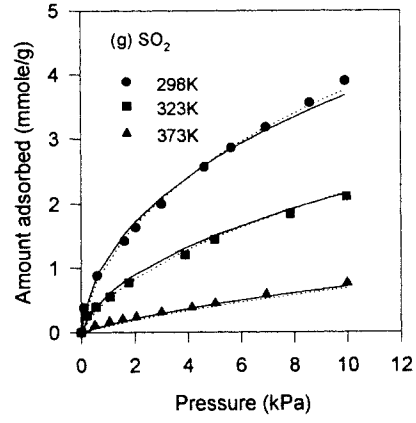

Figure 1. Isotherm fittings for the model equation:

(a) Ethane; (b) propane; (c) butane; (d) benzene; (e) toluene; (f) CO_2; (g) SO_2 (—10-4-3, ··· 10-4 potential).

Table 2a. Optimized Isotherm Parameters for 10-4-3 Potential

	Ethane	Propane	Butane	Benzene	Toluene	CO_2	SO_2
$C^0_{\mu s}$ (mmol/g)	7.480	5.912	4.731	4.866	4.420	9.738	11.81
ϵ^*_k (J/mol)	1.342×10^4	1.627×10^4	2.001×10^4	2.950×10^4	3.056×10^4	1.309×10^4	1.643×10^4
δ (1/K)	1.5×10^{-5}						
E_{mean} (J/mol)	1.963×10^4	2.610×10^4	3.210×10^4	3.781×10^4	4.475×10^4	1.638×10^4	2.371×10^4

Table 2b. Optimized Isotherm Parameters for 10-4 Potential

	Ethane	Propane	Butane	Benzene	Toluene	CO_2	SO_2
$C^0_{\mu s}$ (mmol/g)	7.491	5.904	4.736	4.888	4.512	9.687	12.2
ϵ^*_k (J/mol)	1.513×10^4	1.823×10^4	2.245×10^4	3.282×10^4	3.429×10^4	1.494×10^4	1.771×10^4
δ (1/K)	1.83×10^{-5}						
E_{mean} (J/mol)	2.054×10^4	2.650×10^4	3.264×10^4	4.296×10^4	4.602×10^4	1.824×10^4	2.277×10^4

ics data were collected with slab pellets of two different sizes: 4.4 mm and 2.6 mm full length. For larger particles, three operating temperatures (283 K, 303 K and 333 K) were used, while for smaller particles the experimental temperature was kept at 303 K. The mole fraction of ethane in bulk gas are 5%, 10% and 20% for each temperature.

To extract the kinetic parameters, the optimizations are performed for both models on the experimental data at 303 K on 4.4 mm slab particles. The optimized parameters using 10–4–3 potential are listed in the Table 3, and the simulation results (solid line for FK model, dashed line for HMSD model) and experimental data (dots) are plotted in Figure 4a. It is seen that the FK model adequately describes adsorption as well as desorption kinetics; the long tail effect is well reproduced, because in the finite kinetics model molecules from the high energy site desorb slowly back to the fluid phase due to the high energy barrier. On the other hand, the HMSD model simulates adsorption kinetics well but is inferior in representing the desorption kinetics. Thus, the finite kinetics term cannot be ignored in the description of overall kinetics.

It is imperative to discuss the relative importance of various processes. During the initial stage of the adsorption uptake, the concentration in the adsorbed phase is very low. This will result in two effects:

(1) the surface flux is small because of the dependency of the surface diffusivity on loading (the lower the loading, the lower is the surface diffusivity, hence flux);

(2) the driving force for mass interchange is high due to the large concentration difference between the two phases [Eq. 8].

So, the mass-transfer flux is more influenced by the mass exchange between the two phases. With the progress of adsorption, the surface diffusivity increases due to an increase in the surface loading and the driving force for mass exchange decreases. This results in the FK model exhibiting slower kinetics than the HMSD model at the later stage of the uptake.

In desorption mode, both surface diffusion and finite kinetics play an important role at the beginning, and thus re-

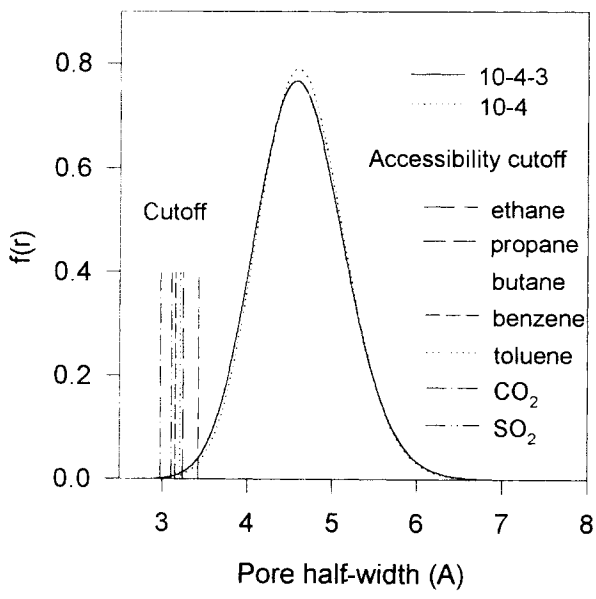

Figure 2. MPSD for Ajax activated carbon and pore accessibility of each species.

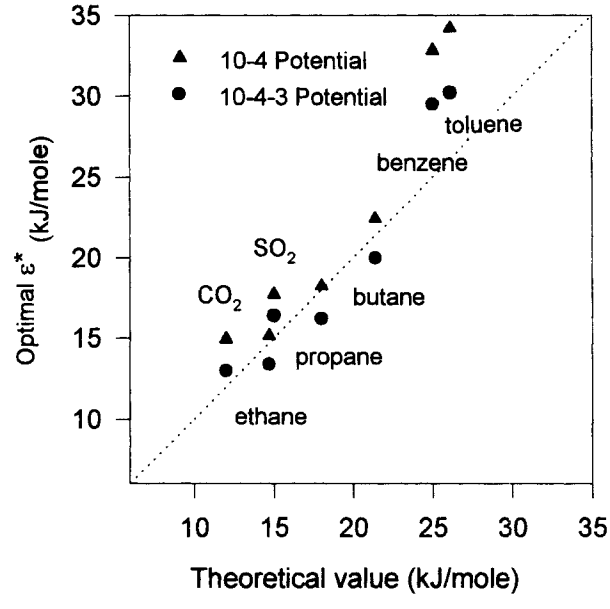

Figure 3. ϵ^*_k for each species against their theoretical values calculated using the parameters from the references (Bird, 1962; Steele, 1974).

Table 3. Kinetics Parameters for Different Adsorbates

		D_p (10^{-6} m^2/s)			$D^0_{\mu\infty}$ (10^{-7})	k_a (10^{-4})	$D^0_{\mu\infty}$ (10^{-7})	
	Potential	283 K	303 K	333 K	m^2/s	L/s/[mol/m^3]	m^2/s (HMSD)	a
Ethane	10-4-3	1.51	1.68	1.96	5.10	0.52	3.06	0.5
	10-4				4.85	0.64	2.81	0.5
Propane	10-4-3	1.20	1.30	1.56	3.60	1.28	2.94	0.5
Butane	10-4-3	1.08	1.14	1.36	5.83	12.6	7.32	0.5
Benzene	10-4-3	1.06	1.08	1.10	4.66	4.71	5.85	0.5
Toluene	10-4-3	0.87	0.86	0.99	4.06	5.01	8.78	0.5
CO_2	10-4-3	2.35	2.60	2.80	7.26	9.85	8.20	0.5
SO_2	10-4-3	1.90	2.10	2.50	3.71	1.16	3.85	0.5

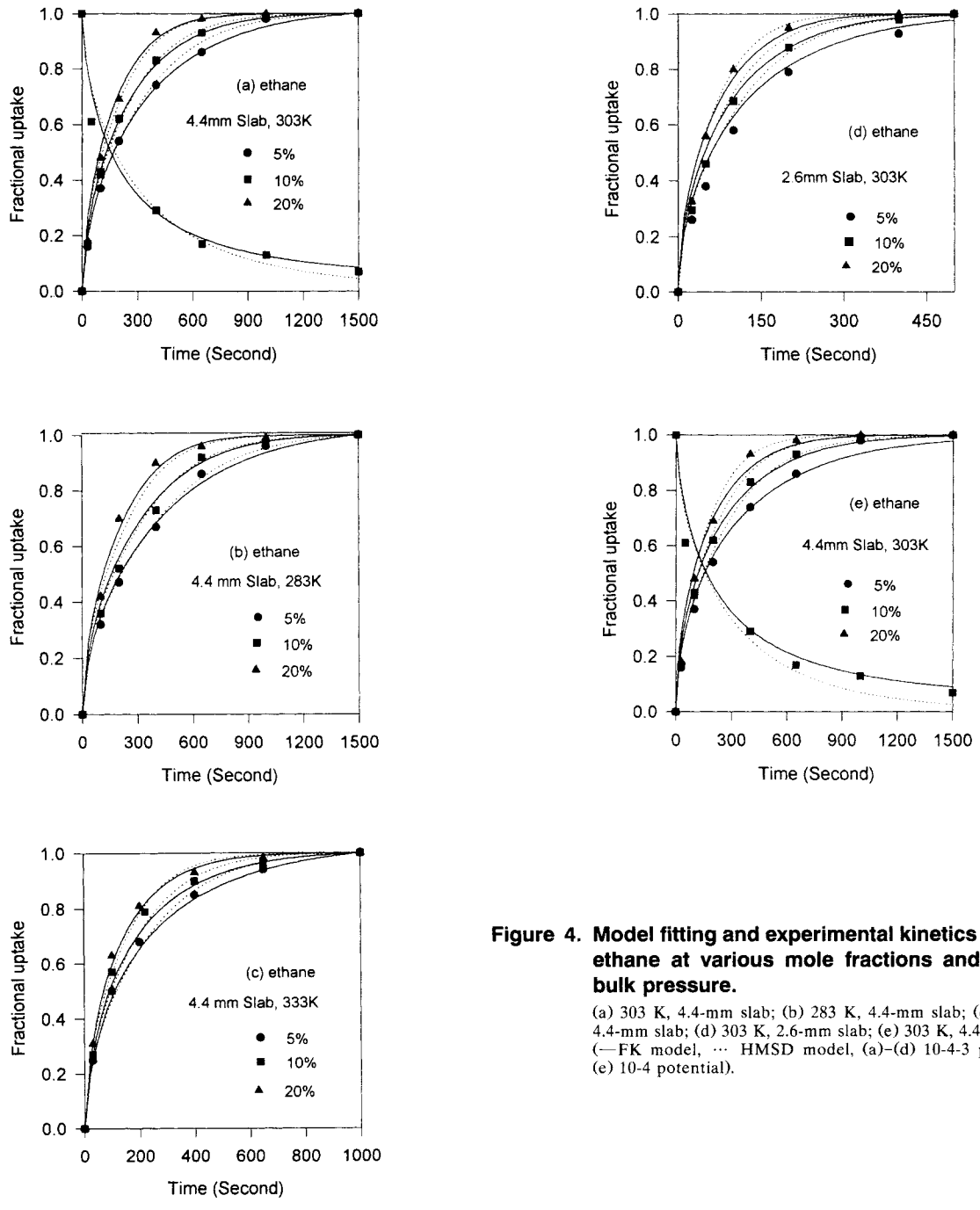

Figure 4. Model fitting and experimental kinetics data of ethane at various mole fractions and 1 atm bulk pressure.

(a) 303 K, 4.4-mm slab; (b) 283 K, 4.4-mm slab; (c) 333 K, 4.4-mm slab; (d) 303 K, 2.6-mm slab; (e) 303 K, 4.4-mm slab (—FK model, ··· HMSD model, (a)–(d) 10-4-3 potential, (e) 10-4 potential).

sult in a sharp drop in desorption curve. However, as the desorption proceeds further, the driving force for finite kinetics decreases very quickly and the long tail in the desorption curve is observed. This tail suggests the importance of the finite kinetics between the two phases.

With the optimal parameters listed in Table 3, we use both models (FK and HMSD) to predict the adsorption kinetics of ethane on the same pellet but at the other two temperatures, 283 K and 303 K. The prediction results from the FK and HMSD models are represented in Figures 4b and 4c by a solid line and a dashed line, respectively. The fittings are excellent for both models, justifying the correct description of temperature dependence in these models. Next, these optimal parameters are employed to simulate the adsorption kinetics on the smaller sized pellets, the 2.6 mm slab particles. The model predictions (solid line and dotted line) and the experimental data (dots) are plotted in Figure 4d, which again shows that both model predictions are in good consistency with the experimental results but the prediction from the FK model is more satisfactory.

As a comparison, the 10-4 potential is also employed to simulate the adsorption kinetics of ethane at 303 K on 4.4 mm slab particles. The model fitting is shown in Figure 4e as a solid line for the FK model and a dotted line for the HMSD model. The optimized parameters are also listed in Table 3. It is seen that the results are comparable with those from 10-4-3 potential, which suggests that the kinetics are not sensitive to the choice of the potential form. The 10-4-3 potential is then used in all subsequent simulations.

Propane. The adsorption kinetics of propane were measured on the same particles and under the same operating conditions as those of ethane. The optimization procedures described earlier for ethane are applied for propane. The optimal results obtained from the fitting of the experimental data at 303 K on a 4.4 mm slab with the models are listed in Table 3. Model fittings and predictions are shown in Figures 5a–5d as lines while experimental data are plotted as symbols. The model fittings and the predictions are all excellent, notably, however, the long tail effect in the desorption curve is described slightly better by the FK model.

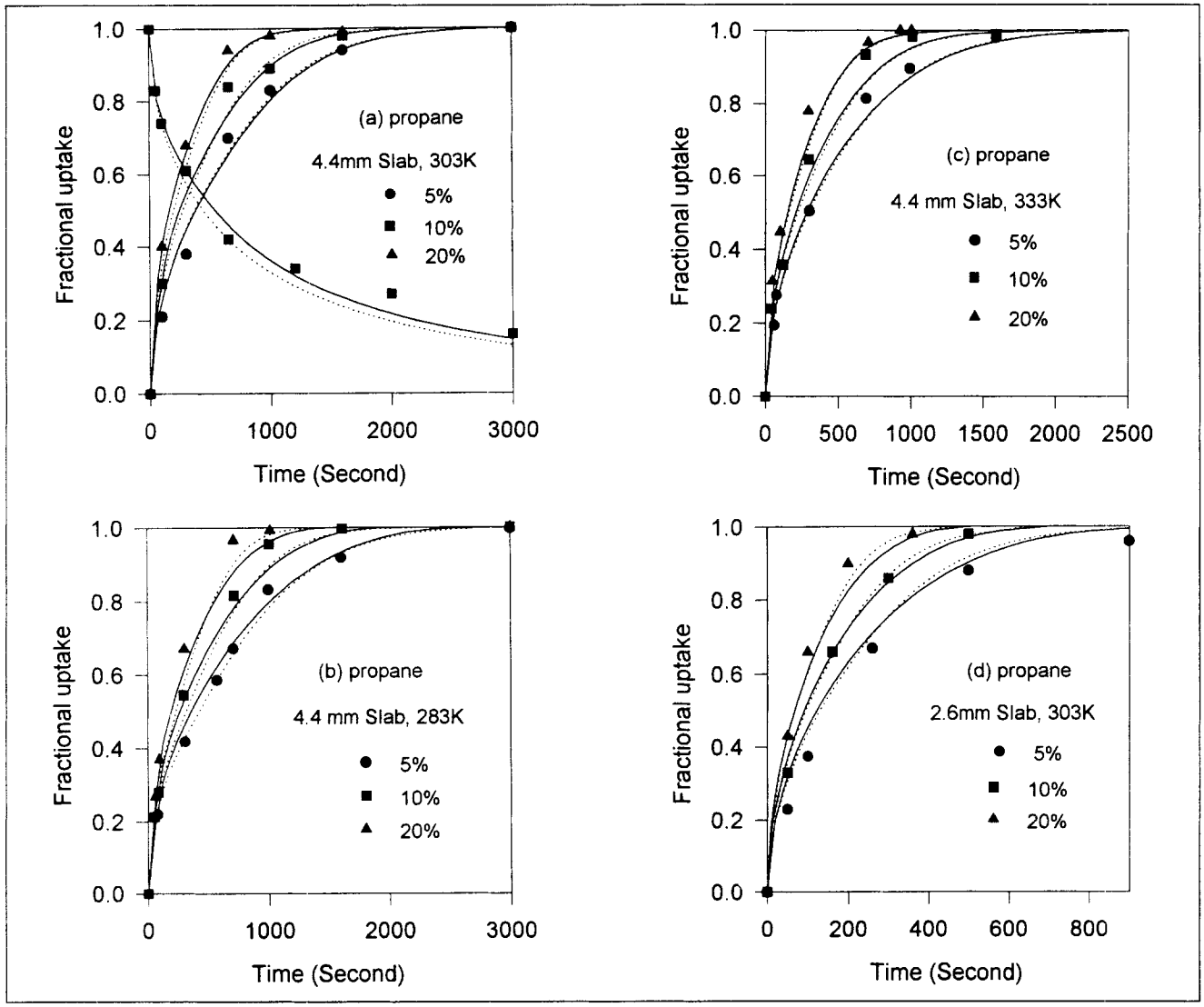

Figure 5. Model fitting and experimental kinetics data of propane at various mole fractions and 1 atm bulk pressure.

(a) 303 K, 4.4-mm slab; (b) 283 K, 4.4-mm slab; (c) 333 K, 4.4-mm slab; (d) 303 K, 2.6-mm slab (—FK model, ··· HMSD model).

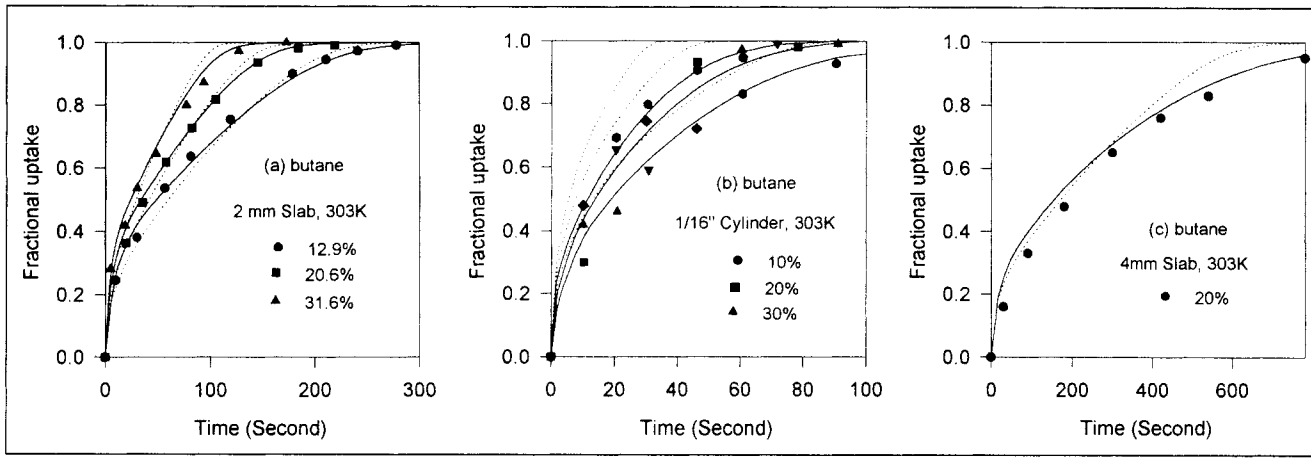

Figure 6. Model fitting and experimental kinetics data of butane at 303 K and 1 atm bulk pressure with various mole fractions.

(a) 1-mm slab; (b) 1/16-in. (1.6-mm) cylinder; (c) 2-mm slab (—FK model, ··· HMSD model).

Butane. The adsorption kinetics experiments of *n*-butane are carried out at the same temperature: 303 K, but on particles with different sizes: 2-mm slab; 4-mm slab; and 1/16-in. (1.6 mm) cylinder. The fitting is carried out with the experimental data of the 2-mm slab with three bulk mole fractions (12.9%, 20.6% and 31.6%). The fitting results are shown in Figure 6a and the optimized kinetics parameters are shown in Table 3.

With the kinetics parameters in Table 3, we use both mathematical models to predict the adsorption kinetics on a 1/16-in. (1.6-mm) cylinder and 4-mm slab particles (Figures 6b and 6c). Here we see that the adsorption kinetics predicted by the FK model is superior to that of the HMSD model, suggesting the great significance of the finite mass interchange on the 1/16-in. (1.6-mm) cylinder. For larger size pellets (4 mm), both models are adequate but the FK model shows its superiority in model prediction.

Benzene and Toluene. To further examine the model's applicability and predictability, the kinetics data of the other class of hydrocarbon, the aromatics, are also employed in our study. The adsorption temperatures are 303 K and 333 K for benzene and 303 K for toluene. The bulk mole fraction are 0.415% and 0.912% for each species. The adsorption kinetics of benzene are collected using the 2-mm full length slab particles while the kinetics of toluene are collected using the 2-mm slab and 1/16 in. (1.6-mm) cylinder. The fittings are shown in Figure 7 for benzene and Figure 8 for toluene. The fittings are excellent for both species, and the optimized parameters are listed in Table 3.

CO_2. The adsorption as well as desorption kinetics of CO_2 were studied on the 6 mm full length slab particle at three

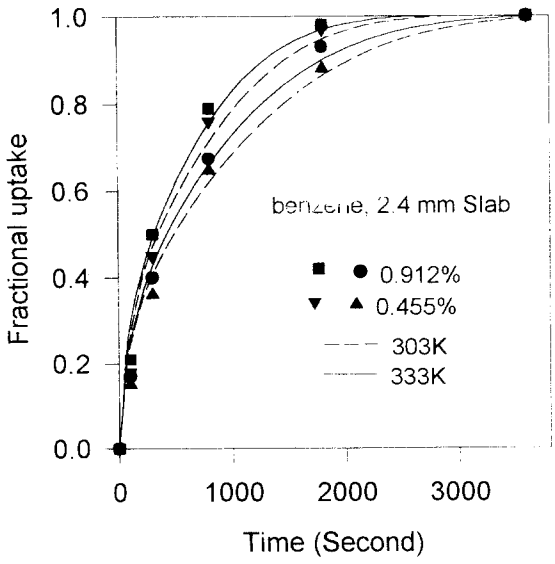

Figure 7. Model fitting and experimental kinetic data of benzene on 2.4-mm slab at different temperatures and mole fractions.

Total gas-phase pressure is 1 atm.

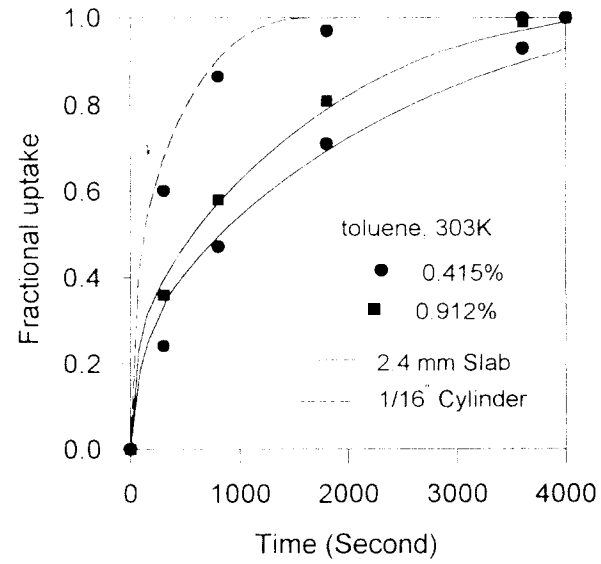

Figure 8. Model fitting and experimental kinetics data of toluene at 303 K on different sized pellets.

Total gas-phase pressure is 1 atm.

temperatures: 298 K, 323 K and 343 K (Gray and Do, 1991). In the adsorption experiment, the particles are exposed to a constant bulk condition of 20% mole fraction of CO_2 and 1 atm total pressure, while in the desorption experiment the particles preequilibrated with the same CO_2 concentration are desorbed in the stream of inert gas. The adsorption kinetics data of CO_2 at three temperatures are chosen for fitting with the mathematical models and extracting the optimized kinetics parameters. The fitting is shown in Figure 9a, and the optimal parameters are listed in Table 3. Again, those optimized results are employed to predict the desorption kinetics on the same particles. We can see in Figure 9b that both models can adequately simulate the adsorption data with the FK model being a better model.

SO_2. To finally test the applicability of the mathematical model, we use the experimental data of SO_2 on Ajax activated carbon (Gray and Do, 1990). The pellets used in the experiment are the 4-mm full-length slab particle and the experiments are carried out at three different temperatures (298 K, 323 K and 373 K) with the bulk mole fraction being 0.5%, 2% and 5% for each temperature. The optimizations are first performed for the desorption data at 298 K with the three bulk mole fractions. The fittings are shown graphically in Figure 10a and the optimized parameters are listed in Table 3. The fittings from both models are seen to be good.

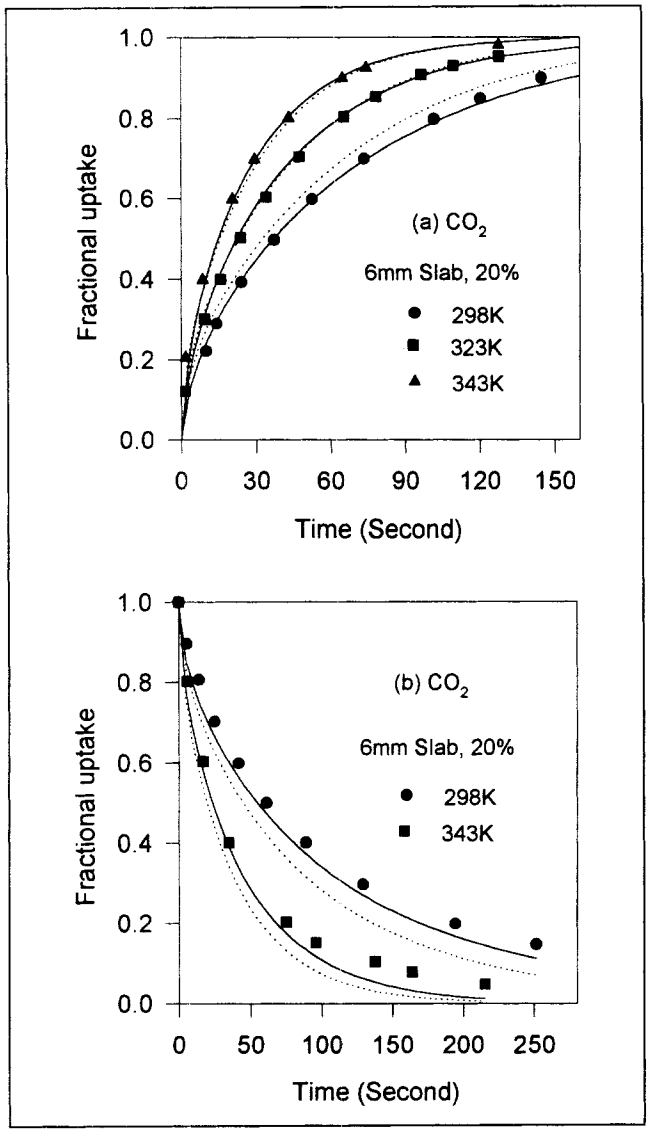

Figure 9. Model fitting and experimental kinetics data of CO_2 on 6-mm slab particle at different temperatures.

Total gas-phase pressure is 1 atm. (a) Adsorption; (b) desorption (—FK model, ··· HMSD Model).

The optimized parameters are then used to predict the desorption kinetics at two other temperatures: 283 K and 373 K. The predictions from both models are shown in Figure 10b, where we can see the excellent prediction of the long tail phenomenon is presented by the FK model. The HMSD model, on the other hand, predicts faster desorption kinetics at either temperature than this model does. Thus, the superiority of this model is again demonstrated. Finally, the parameters are employed to simulate the adsorption kinetics at three different temperatures (Figure 10c). The model predictions from both models are reasonably good.

Discussion of the Optimized Parameters. The mathematical model has been tested successfully with the extensive adsorption kinetics data of seven adsorbates on activated carbon. For the FK model, the two kinetics parameters extracted from the optimization are the surface diffusivity at zero loading and infinite temperature $D^0_{\mu\infty}$ (m^2/s) and the adsorption rate constant k_a [$1/s(mol/m^2)$]. It is important that we discuss these extracted parameters in this section.

Surface Diffusivity at Zero Loading and Infinite Temperature $D^0_{\mu\infty}$. The parameter $D^0_{\mu\infty}$ represents the mobility of the adsorbate molecule on the surface at zero loading condition and at infinite temperature. Because it represents the mobility of the molecule at infinite temperature and at zero loading, it is reasonable to expect that this parameter is associated with the solid surface properties. The extracted values of $D^0_{\mu\infty}$ of seven adsorbates from the FK model are plotted in Figure 11 (squares), and we note that within experimental error these values are of the same order of magnitude with an average of 4.9×10^{-7} m^2/s, except the value of $D^0_{\mu\infty}$ for CO_2 is a bit larger than the average. This seems to support our contention that $D^0_{\mu\infty}$ is intrinsic and only specific to the adsorbent concerned. It may have a weak dependence on the molecular weight. Further fundamental work is needed to test this hypothesis. Compared with the value of the same variable (the average $D^0_{\mu\infty}\approx 9\times10^{-7}$ m^2/s) obtained from our previous study (Do and Wang, 1997), the results in this study are a bit smaller. This is mainly attributed to the way we drive the MPSD in which the size difference is taken into account, and the choice of 10-4-3 potential. The optimized values of $D^0_{\mu\infty}$ of seven species from the HMSD model are also plotted in Figure 11 (circles), and one can see that these values are more scattered than the values from the FK model, the average value of which is 5.38×10^{-7} m^2/s. The more scattering of the diffusivities of the HMSD model may point to the FK model being a better model.

k_a. The rate constant for adsorption k_a measures the finite mass interchange between gas and adsorbed phase in the overall uptake. The larger this parameter, the faster the gas and adsorbed phase will reach equilibrium. As shown in previous analysis and simulations, it is an important factor in describing the sorption kinetics in activated carbon. Gener-

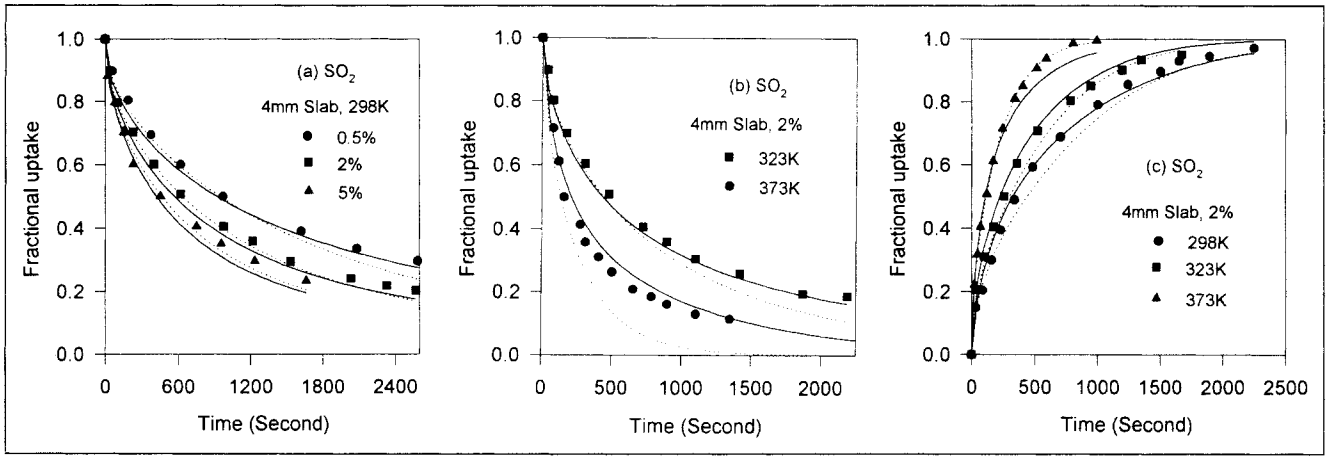

Figure 10. Model fitting and experimental kinetics data of SO_2 on 4-mm slab particle at different temperatures.

Total gas-phase pressure is 1 atm. (a) Desorption; (b) desorption (c) adsorption. (—FK model, ··· HMSD model).

ally speaking, the mass interchange plays a more important role at the initial stage of uptake processes, because the driving force for mass transfer is the largest at this stage of uptake. The simulation results also suggest that, for adsorbates of the same family, this parameter increases with the increase of isotherm curvature (adsorption affinity). For adsorbates of different families, however, this trend is not so obvious. Compared with $D^0_{\mu\infty}$, the optimized values of k_a for each species are more scattered, but they are in the order of 10^{-4} [1/s/(mol/m^3)], showing a general trend of increase with the increase of the interaction energy between adsorbate and solid, except some deviation is observed for that of CO_2. This abnormality is understandable since our model is strictly developed for nonpolar adsorbates like hydrocarbons, and it is possible that the other adsorbate-surface interactions induced by the polarity also play some role in the overall adsorption kinetics.

Optimization Procedure. Although the FK model has two kinetics parameters to be optimized, its convergence is generally good. However, if we perform optimization for the adsorption kinetics data at one temperature with several bulk gas concentrations, special attention is needed to locate the optimal values as the goodness of fit only improves marginally even though the set of parameter $D^0_{\mu\infty}$ and k_a may change significantly. This constitutes some difficulties since different combinations of $D^0_{\mu\infty}$ and k_a can simulate the data within the experimental error. To overcome this problem, it is recommended that optimization be performed for adsorption data and desorption data simultaneously, or in case the desorption data is unavailable, the adsorption data on different sized pellets or at different temperatures are optimized together. In either case, the final convergence is ensured.

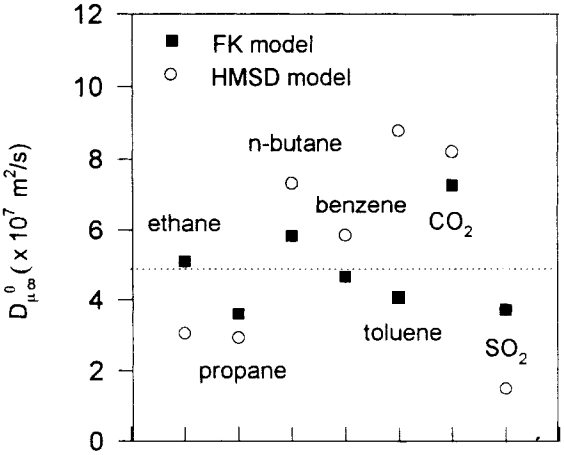

Figure 11. Surface diffusivity at zero loading and infinite temperature $D^0_{\mu\infty}$ of each species.

Conclusion

We have proposed and tested a new mathematical model for adsorption kinetics, which is based on the structural characteristics of activated carbon. This model incorpates three mass-transfer processes in the overall sorption kinetics: pore diffusion, surface diffusion, and the finite mass interchange between the gas and adsorbed phases. The driving force for surface diffusion is chemical potential gradient and the mass interchange rate is described by the Langmuir kinetics. The pore-size distribution of the slit-shaped micropores is considered as the main source of heterogeneity which governs the adsorption equilibria and kinetics through the dispersive force represented by the Lennard-Jones potential theory. This distribution is obtained by fitting the multiple-temperatured isotherm data of many adsorbates simultaneously and is employed to study the sorption kinetics of ethane, propane, butane, benzene, toluene, carbon dioxide, and sulfur dioxide over a range of operating conditions and parameters. The model fittings and predictions are found to be excellent in general, and in particular the model is able to predict the long tail behavior observed in desorption mode. Such long tail behavior has been unable to be accounted for by any previous models, and this has testified for the potential applicability of the model proposed in this article.

The implications of the model are also discussed. One of the special cases for this model, the HMSD model proposed by Do and Hu (1993), is also employed in the simulation as a reference to study the role of the finite kinetics in the overall

adsorption process. It is found that finite kinetics play an important role in the overall kinetics, especially at the initial stage of adsorption process, and it cannot be neglected in the description of the sorption kinetics on activated carbon.

Acknowledgment

The support from the Australia Research Council (ARC) is gratefully acknowledged.

Notation

b_0 = adsorption affinity at zero energy level, $1/(\text{mol/m}^3)$
C^* = hypothetical gas-phase concentration, (mol/m^3)
D_μ = surface diffusivity, m^2/s
J_P = pore flux, $\text{mol/m}^2/\text{s}$
$k_{d,\infty}$ = desorption rate constant at zero energy level, s^{-1}
k_m = film mass-transfer coefficient, m^{-1}
$L(r)$ = mobility at pore with half width r
M = molecular weight
R_g = gas constant
t = time, (s)
X = reduced particle coordinate
Y = dimensionless gas-phase concentration
Y_μ = dimensionless adsorbed-phase concentration
β = affinity parameter, $\text{m}^3\ \text{mol}^{-1}\ (\text{g}\cdot\text{K/mol})^{1/2}$
ϵ = particle porosity
σ_{sk} = collision diameter between the solid and the fluid molecules, Å
ϵ_{sk} = cross interaction energy minimum, J/mol
$\varphi_k(z,r)$ = potential at distance z in pore with radius r, J/mol

Literature Cited

Bird, R. B., W. E. Stewart, and E. N. Lightfoot, *Transport Phenomena*, Wiley, New York (1962).

Do, D. D., "A Model for Surface Diffusion of Ethane and Propane in Activated Carbon," *Chem. Eng. Sci.*, **51**, 4145 (1996).

Do, D. D., "Dynamics of Adsorption in Heterogeneous Solids," in *Equilibria and Dynamics of Gas Adsorption on Heterogeneous Solid Surfaces*, W. Rudzinski, W. Steele, and G. Zgrablich, eds., Elsevier, Amsterdam (1997).

Do, D. D., and X. Hu, "An Energy Distributed Model for Adsorption Kinetics in Large Heterogeneous Microporous Particle," *Chem. Eng. Sci.*, **48**, 2119 (1993).

Do, D. D., and H. D. Do, "A New Adsorption Isotherm for Heterogeneous Adsorbent Based on the Isosteric Heat as a Function of Loading," *Chem. Eng. Sci.*, **52**, 297 (1996).

Do, D. D., and K. Wang, "A New Model for the Description of Sorption Kinetics in Heterogeneous Activated Carbon," *Carbon*, in press (1997).

Everett, D. H., and J. C. Powl, "Adsorption in Slit-Like and Cylindrical Micropores in the Henry's Law Region," *J. Chem. Soc. Farad. Trans.*, **72**, 619 (1976).

Gray, P., and D. D. Do, "Adsorption and Desorption of Dynamics of Sulfur Dioxide on a Large Activated Carbon Particle," *Chem. Eng. Commun.*, **96**, 141 (1990).

Gray, P., and D. D. Do, "Dynamics of Carbon Dioxide Sorption on Activated Carbon Particle," *AIChE J.*, **37**, 1027 (1991).

Hu, X., and D. D. Do, "Role of Energy Distribution in Multicomponent Sorption Kinetics in Bidispersed Solid," *AIChE J.*, **39**, 1628 (1993).

Hu, X., and D. D. Do, "Effect of Surface Heterogeneity on the Sorption Kinetics of Gases in Activated Carbon, Pore Size Distribution vs. Energy Distribution," *Langmuir*, **10**, 3296 (1994).

Innes, R. W., J. R. Fryer, and H. F. Stoeckli, "On the Correlation between Micropore Distribution Obtained from Molecular Probes and from High Resolution Electron Microscopy," *Carbon*, **27**, 71 (1989).

Jagiello, J., "Characterization of Microporous Carbons Using Adsorption at Near Ambient Temperature," *Langmuir*, **12**, 2837 (1996).

Myers, A. L., "Adsorption of Pure Gases and their Mixtures on Heterogeneous Surface," *Fundamentals of Adsorption*, Engineering Foundation, New York (1984).

Russell, B. P., and M. D. LeVan, "Pore Size Distribution of BPL Activated Carbon Determined by Different Methods," *Carbon*, **32**, 845 (1994).

Ruthven, D. M., *Principles of Adsorption and Adsorption Process*, Wiley, New York (1984).

Steele, W. A., *The Interaction of Gases with Solid Surface*, Pergamon, Oxford (1974).

Yang, R. T., *Gas Separation by Adsorption Processes*, Butterworth, Boston (1987).

Appendix

The nondimensional model equations for Eqs. 14 and 15 are

$$\sigma\frac{\partial Y}{\partial\tau}+\sigma_\mu\frac{\partial}{\partial\tau}\left\{\int_{x_{\min}}^{x_{\max}}Y_\mu(x)f(x)dx\right\}=\eta\frac{1}{X^s}\frac{\partial}{\partial X}\left\{X^s\frac{\partial Y}{\partial X}\right\}$$
$$+\delta\frac{1}{X^s}\frac{\partial}{\partial X}\left\{X^s\int_{x_{\min}}^{x_{\max}}H(x)\frac{C_R}{C_R-Y_\mu(x)}\frac{\partial Y_\mu(x)}{\partial X}f(x)dx\right\} \tag{A1}$$

Table A1. Nondimensional Groups and Parameters

$$Y=\frac{C}{C_0}\qquad Y_\mu(x)=\frac{C_\mu(x)}{C_{\mu 0}}\qquad C_R=\frac{C_{\mu s}}{C_{\mu 0}}\qquad X=\frac{Z}{R}\qquad x=\frac{r}{\sigma_{sk}}$$

$$\bar{x}=\frac{\gamma+1}{q\sigma_{sk}}\qquad e(x)=\frac{E(x)}{R_gT}\qquad \lambda=C_0b_0\exp[e(x)]$$

$$H(x)=\exp\{a[e(\bar{x})-e(x)]\}\qquad H_k(x)=\exp[e(\bar{x})-e(x)]$$

$$\sigma=\frac{\epsilon C_0}{\epsilon C_0+(1-\epsilon)C_{\mu 0}}$$

$$\sigma_\mu=\frac{(1-\epsilon)C_{\mu 0}}{\epsilon C_0+(1-\epsilon)C_{\mu 0}}$$

$$\eta=\frac{\epsilon D_pC_0}{\epsilon D_pC_0+(1-\epsilon)D^0_{\mu\infty}\exp[-ae(\bar{x})]C_{\mu 0}}$$

$$\delta=\frac{(1-\epsilon)D^0_{\mu\infty}\exp[-ae(\bar{x})]C_{\mu 0}}{\epsilon D_pC_0+(1-\epsilon)D^0_{\mu\infty}\exp[-ae(\bar{x})]C_{\mu 0}}$$

$$\tau=\frac{\{\epsilon D_pC_0+(1-\epsilon)D^0_{\mu\infty}\exp[-ae(\bar{x})]C_{\mu 0}\}t}{[\epsilon C_0+(1-\epsilon)C_{\mu 0}]R^2}$$

$$\gamma=\frac{[\epsilon C_0+(1-\epsilon)C_{\mu 0}]D^0_{\mu\infty}\exp[-ae(\bar{x})]}{\epsilon D_pC_0+(1-\epsilon)D^0_{\mu\infty}\exp[-ae(\bar{x})]C_{\mu 0}}$$

$$\psi=\frac{[\epsilon C_0+(1-\epsilon)C_{\mu 0}]R^2k_aC_0}{\epsilon D_pC_0+(1-\epsilon)D^0_{\mu\infty}\exp[-ae(\bar{x})]C_{\mu 0}}$$

$$\zeta=\frac{[\epsilon C_0+(1-\epsilon)C_{\mu 0}]R^2k_{d,\infty}\exp[-e(\bar{x})]}{\epsilon D_pC_0+(1-\epsilon)D^0_{\mu\infty}\exp[-ae(\bar{x})]C_{\mu 0}}$$

$$\text{Bi}=\frac{k_mRC_0}{\epsilon D_pC_0+(1-\epsilon)D^0_{\mu\infty}\exp[-ae(\bar{x})]C_{\mu 0}}$$

$$\frac{\partial Y\mu(x)}{\partial \tau} = \gamma \frac{1}{X^s} \frac{\partial}{\partial X} \left\{ X^s H(x) \frac{C_R}{C_R - Y_\mu(x) z} \frac{\partial Y_\mu(x)}{\partial X} \right\}$$
$$+ \psi Y [C_R - Y_\mu(x)] - \zeta \times H_k(x) Y_\mu(x)$$
$$= \gamma \frac{1}{X^s} \frac{\partial}{\partial X} \left\{ X^s H(x) \frac{C_R}{C_R - Y_\mu(x)} \frac{\partial Y_\mu(x)}{\partial X} \right\}$$
$$+ [\psi Y + \zeta \times H_K(x)] \left\{ C_R \frac{\lambda(x) Y}{1 + \lambda(x) Y} - Y_\mu(x) \right\} \quad \text{(A2)}$$

The corresponding boundary conditions for above equations are

$$X = 0, \qquad \eta \frac{\partial Y}{\partial X} = 0$$

$$X = 1, \qquad \eta \frac{\partial Y}{\partial X} + \delta \left\{ \int_{x_{\min}}^{x_{\max}} H(x) \frac{C_R}{C_R - Y_\mu(x)} \frac{\partial Y_\mu(x)}{\partial X} f(x) dx \right\}$$
$$= Bi(Y_b - Y)$$

$$\tau = 0, \qquad Y_\mu = C_R \int_{x_{\min}}^{x_{\min}} \frac{Y_0 \lambda(x)}{1 + Y_0 \lambda(x)} f(x) dx \quad \text{(A3)}$$

The corresponding nondimensional groups and parameters are listed in Table A1.

Manuscript received June 12, 1997, and revision received Sept. 18, 1997.